Available online at www.sciencedirect.com
SCIENCE DIRECT®
Polymer 45 (2004) 1401–1411
polymer
www.elsevier.com/locate/polymer

Molecular modelling of the uniaxial deformation of amorphous polyethylene terephthalate

Mathieu Roberge, Robert E. Prud'homme, Josée Brisson*

Department of chemistry and Centre de recherche en science et ingénierie des macromolécules (CERSIM), Faculté des sciences et de génie, Université Laval, Pavillon Vachon, Québec, Canada G1K 7P4

Received 5 February 2003; received in revised form 22 April 2003; accepted 29 April 2003

Abstract

Deformation of polyethylene terephthalate, PET, was simulated using atomistic molecular dynamics using a Parrinello–Rahman constant-stress constant-temperature algorithm under periodic boundary conditions. The evolution in *trans* and *gauche* populations is in good agreement with experimental data reported in the literature: In the isotropic model, approximately 15% *trans* angles are found, and the *trans* population increases up to a value of 50% at a draw ratio λ of 3.2. There is a gradual increase in the orientation function of the aromatic cycles, $\langle P_2(\cos\theta)\rangle_c$, with λ, but the values are higher than those reported in the literature, due to the absence of relaxation in the simulation. Moreover, the orientation of *trans* segments was found to be high, while the orientation of *gauche* segments was non negligible. A good agreement was found with the rubber elasticity model up to a λ of 2.0, as was the case for previous polyvinyl phenol simulations. Simulated data fit well with the aggregate model in a broad range, for 1.0 λ 5.0, contrarily to the case of poly(vinyl phenol), where the aggregate model predicted much higher orientation values that those obtained via molecular modelling simulations. This difference is attributed to the different rigidities of the chain backbones. Simulations were found in good agreement with those performed by Zhou, Nicholson, Davies and Ward, using a different deformation simulation approach, both in terms of orientation of aromatic rings and of conformer evolution during deformation.

Keywords: Orientation; Modelling; Uniaxial deformation

1. Introduction

The orientation of polymers, both in their pure state and in blends, influences markedly most of their properties, including mechanical, optical, and electrical properties. Many techniques have been developed to induce orientation during processing, such as fiber drawing, roll-drawing, pultrusion, etc. Considerable effort has also been made to develop characterization techniques for orientation, with the aim of better understanding and controlling this phenomenon. In our group, studies have focussed on the processes occurring at a molecular level during polymer deformation and relaxation.

More recently, we have turned to atomistic molecular modeling simulations for new insights into this phenomenon. A first report was published on poly(vinyl phenol) (PVPh) deformation using a Parrinello–Rahman molecular dynamics deformation algorithm [1]. In these simulations, *trans* segments orient considerably more than *gauche* segments, and the *trans* population increases upon deformation. It was however impossible to compare these observations to experimental data, as no infrared vibration specific to *trans* or *gauche* moieties are known for PVPh.

For poly(ethylene terephthalate) (PET), on the other hand, *gauche* and *trans*-specific wagging vibrations of the glycol units are well known. We have previously studied the orientation of this polymer using X-ray diffraction, infrared dichroism [2], birefringence [3] and polarisation–modulation infrared linear dichroism [4].

In the present article, simulations of deformation-induced orientation of PET will be discussed in terms of orientation and conformation of chain segments and compared to experimental data. Comparison will also be made with previous isotropic models of the amorphous phase [5], oriented models created using a Monte–Carlo rotational isomeric state approach [6] as well as a molecular dynamics simulation performed by sequential molecular dynamics

* Corresponding author. Tel. +1-418-656-3536; fax: +1-418-656-7916.
E-mail address: josee.brisson@chm.ulaval.ca (J. Brisson).

0032-3861/$ - see front matter © 2003 Elsevier Ltd. All rights reserved.
doi:10.1016/j.polymer.2003.04.005

steps at constant number of atoms, volume and temperature (NVT) and unit cell deformation steps for short 10-mer PET chains [7].

2. Experimental section

Modelling calculations were conducted either on a SGI Indigo workstation, or on one processor of a Origin-2000 server using InsightII, Discover_3, Polymerizer and Amorphous_Cell modules from Accelrys. The pcff forcefield [8,9] was used throughout. This forcefield has been explicitly parametrized for aromatic esters [10]. It includes a Morse potential for bond deformation energies, an harmonic potential for angle deformation, a Fourier series for torsion angle deformation, a Lennard–Jones 6–12 potential for van der Waals interactions and an electrostatic energy term. Partial charges are included in the forcefield. Cross-terms were not included. The non-bond potential cut-off distance was set to 9.5 Å and a quintic spline attenuation function was used from 9.5 to 10.0 Å throughout. Pair-list updates were performed whenever any atom moved more than half this buffer width.

2.1. Construction of amorphous phase model

The construction of five isotropic amorphous phase models was performed under periodic boundary conditions and minimum image convention by the scanning method proposed by Meirovitch [11]. Catenation problems were encountered: as new repeat units were added to the chain under construction, the chain passed in some instances in the center of aromatic moities. Alternatively, chain construction could lead to the creation of two intertwined cycles, which led to model construction failure. In order to alleviate these problems, the model was created at an initial density of 0.6 g cm^{-3} and the density was then brought to the desired value of 1.133 g cm^{-3} using NPT molecular dynamics until the desired density was approached. Final density was fixed by slightly changing the unit cell dimensions to a cubic cell with $a = 4.08$ nm. Many different growth schemes were tested, and the one leading to the lowest final energies was selected for final model deformation studies. In this scheme, six bonds were added at a time, which was the maximum allowed by the software used, and a lookahead of 6 bonds was used. Lower number of bonds or of lookaheads led to high-energy models or to more repeated construction failures related to catenation problems. Because of the high number of lookahead used, torsion angle selection was performed on a random sampling basis instead of the more usual rotational isomeric state or energy-based criteria.

The final molar mass was 54 600 g mol^{-1}, which corresponds to 285 $C_{10}O_4H_8$ repeat units and a total number of atoms of 6272 (which includes two hydrogen atoms attached at chain ends). When considering the experimental molecular weight between entanglements M_e of 1750 g mol^{-1} [18], this simulated chain length corresponds to 31 Kuhn segments. Hydrogen atoms were explicitly included in the calculations. The initial models were relaxed using 5000 dynamics steps with a Δt of 1 fs at a temperature of 2000 K using the Verlet velocity integration algorithm under periodic boundary conditions and constant number of particles, volume and temperature (NVT) conditions. Density-dependent tail corrections were applied as described in Ref. [12] for selected simulations, and were found to have no significant effect on the final orientation and conformation population. These calculations were followed by minimisation using a maximum of 1000 steepest descent steps (convergence criterion of 100 kcal/Å) and a maximum of 10 000 conjugate gradients steps (convergence criterion of 1 kcal/Å). Initial $\langle P_2(\cos\theta)\rangle$ orientation values were of 0.00 in all directions. Of the five initial models, three yielded reasonably low energies and were catenation-free.

2.2. Dynamic simulation of the deformation

Dynamic simulation of the deformation was carried out under periodic boundary conditions with the minimum image convention and constant number of particles, stress and temperature (NST) using the Parrinello–Rahman algorithm [14], in which a user-defined cell mass, w, was varied from 10 to 100. The Verlet velocity integration scheme was used with integration steps of 1 fs. Temperature was controlled by velocity scaling, and temperature rescaling was performed whenever the instantaneous temperature deviated from the target value by more than 10 K. Constant symmetrical stress matrix with non-diagonal terms equal to zero were used in all cases. For deformations along the x direction, S_{yy} was always equal to S_{zz} and lower or equal to $-S_{xx}$, while the other matrix components were set to zero. Similar calculations were performed along the y and z axes of the three initially build amorphous models. Unless otherwise stated, deformations were conducted at 25 °C, $S_{xx} = 0.5$ GPa, $S_{yy} = -0.5$ GPa, density = 1.335 g cm^{-1} and $w = 20$. Deformations were also performed at temperatures ranging from 25 to 355 °C. Temperature was controlled by velocity scaling, and temperature rescaling performed under the same conditions as during equilibration. A few selected runs were performed using the Nosé method with Q values of 0.1, 0.25, 0.5 and 1.0 and a time step of.25–0.5 fs and with the Anderson temperature control scheme using a collision rate of 1 with a timestep of 1 fs. Selected deformed cells were also allowed to relax after deformation under NVT conditions, while maintaining the same temperature as the drawing procedure using a velocity rescaling method for 20, 000 fs. A more thorough description of the deformation and relaxation procedures appears in Ref. [1].

3. Results and discussion

3.1. Construction and validation of the initial amorphous phase cell

The construction of the initial amorphous cell, although still posing minor problems with polymers bearing aromatic groups, is nevertheless well established. As proposed in the pioneering work of Theodorou and Suter on polypropylene [14], a limited portion of the amorphous phase is created in a box, which is surrounded by boxes bearing the same content, as in a crystalline phase. This offers the advantage of reproducing correctly the molecular surroundings of the polymer, but induces medium-range symmetry, and this model is, therefore, limited to simulations of processes occurring at the molecular level.

For orientation studies, molecular weight is of particular importance. In this case, it was chosen well above M_e, the molecular weight between chain entanglement. Aharoni [18] has reported a value of M_e of 1 750 g mol^{-1} for PET and n_e, the number of repeat units between entanglements, is therefore, approximately 9. The behaviour of the model should therefore be that of an entangled network. This molecular weight is also considerably higher than that of the PET amorphous phases previously constructed [5,7] which were made of 10 and 60 repeat units, corresponding to 1920 and 11520 g mol^{-1}, respectively.

An additional difficulty in the choice of the chain length is the possibility of having finite size effects. In this particular case, the pertinent correlation length should be that corresponding to the distance between entanglements. The length of Kuhn segments can be defined as:

$$L_k = \langle r_0 \rangle^2 / r_{\text{contour}},$$

where $\langle r_0 \rangle^2$ is the square of the average end-to-end distance and r_{contour} is the contour length of the chain. This is estimated as being of 1.07 nm for each repeat unit. Using the experimental values of $\langle r_0 \rangle^2/M$ measurements, which vary from 0.084 to 0.104 nm mol g^{-1}, the length of a Kuhn segment can be estimated as being of 1.5–1.7 nm. This yields a ratio of distance between entanglements to box size of 0.37–0.42 for the isotropic model. It is therefore, proposed that finite size effects should be minimal in the present case.

Validity of the model was verified using various parameters. Calculations of intermolecular radial distribution function $g(r)$ using the model gave a smooth curve without prominent peaks. The intramolecular $g(r)$ yielded, as expected, peaks corresponding to normal intergroup distances. The average calculated radius of gyration, reported as $\langle r_0 \rangle^2/M$, of the three constructed models is 0.9 ± 0.4 Å^2 mol g with a confidence level of 95%, in agreement with values in the literature, which range from 0.844 [15,16] to 0.949 Å^2 mol g [17,18]. Likewise, the solubility parameter calculated from the model is 19.5 ± 0.7 MPa$^{1/2}$, in agreement with the value of 21.4 MPa$^{1/2}$ reported in the literature [19].

For the O–C–C–O glycol moiety, percentages of *trans* and *gauche* angles in the isotropic model were found to be 15% *trans*, 61% *gauche* and 24% non-*trans*–non-*gauche* angles when defining a *gauche* angle as having an absolute value of 60 ± 20°, and *trans* angle at 180 ± 20°. When considering only two categories of angles, *trans* and non-*trans*, the non-*trans* number reaches 85%. These values are in agreement with those determined from transmission infrared [20–23], specular reflexion infrared [24] or Raman spectroscopy [25] which range from 75 to 88% *gauche* angles. This agreement may appear somewhat surprising since *gauche* conformers are defined as having an energy one to two kcal/mol higher than *trans* conformers for an isolated repeat unit in the forcefield used. In the usual unit cell construction technique proposed by Theodorou and Suter, each bond is added one at a time, following probabilities based on energy considerations, as reflected by the rotational isomeric state statistics. This works well when the repeat unit possesses a small number of backbone bonds. In the case of PET, however, the repeat unit is composed of ten backbone bonds. Addition of one bond at a time invariably results in failure during the cell construction due to catenation problems.

Therefore, the Meirovitch scanning technique was used, where more than one bond is added at a time, as described in the Section 2. Possible conformation states are calculated on the basis of the torsional potentials and of the number of bonds which will be added in the next step, which are called lookahead bonds. In the present study, it was found to be essential to raise the number of lookahead bonds to 6 before a reasonable cell was constructed successfully. In this case, the number of lookahead bonds is too large to calculate probabilities based on energy, and a random sampling is performed instead, such that cell construction is driven more by interchain interactions than by internal energy considerations. It is proposed that this allows the small energy difference between *trans* and *gauche* conformers, as defined in the force field, to be counterbalanced by interchain energy, thus leading to a chain conformation remarkably similar to that reported experimentally for the amorphous phase of PET. It is also noteworthy that the unit cell construction reported by Zhou, Nicholson, Davies and Ward [7] led to a value of 25 ± 5% *trans* angles, while keeping the torsion angle selection energy-based, a value which is comparable to our own value of 15%, the difference probably stemming from specific criteria used for defining a *trans* angle in each study.

3.2. Deformation

In the present work, the Parinello–Rahman dynamic simulation technique was used to simulate deformation as was the case in a previous deformation simulation of PVPh [1]. Contrarily to the majority of deformation simulations,

mechanical property calculations are not sought, the focus being placed instead on the deformation mechanism of the chain, as explored via changes in conformer population and orientation. This simulation technique nevertheless differs in many ways from the actual macroscopic experiments, and these differences must be kept in mind when comparing the simulations to experimental data.

First, this technique uses a constant stress scheme, and is therefore, close to a creep deformation. As can be seen in Fig. 1, which reports the draw ratio λ as a function of time, the deformation is gradual and follows, as expected in creep, a non-linear function, reaching a plateau near $\lambda = 2.0$ for a stress of 0.5 GPa. As the maximum attainable deformation is related to the stress applied, in order to reach higher draw ratios, some simulations were done at higher stresses. Experimentally, most studies dealing with uniaxial orientation are performed at constant deformation rates, which means that stress increases as the material becomes more and more oriented and, therefore, harder and harder to deform. This yields a linear relationship between draw ratio λ and time. Although this should be kept in mind when comparing experimental data to the present simulations, the present simulation can nevertheless help us to gain a better understanding of the deformation process, especially at low deformation ratios, where both creep and constant rate deformation yield a linear relationship for draw ratio versus time.

Second, experimentally, stress is applied to sample extremities. Propagation throughout the sample occurs through chains. Junction points or entanglements are generally accepted as playing a key role in this process, and are the basis of the rubber elasticity theory. In the present model, stress is applied to the polymer via deformation of the cell which defines periodic boundary conditions. The rate at which this change is applied is modulated by a 'cell mass' which can be though of as the mass of a piston applying stress on the cell. The lower this cell mass, the faster the stress is actually transferred to the system, and the faster deformation proceeds. If too low a cell mass is used, however, the system does not have time to readjust, abnormally high energies are observed and the simulation fails. Too high a cell mass simply increases computation time without any simulation improvement.

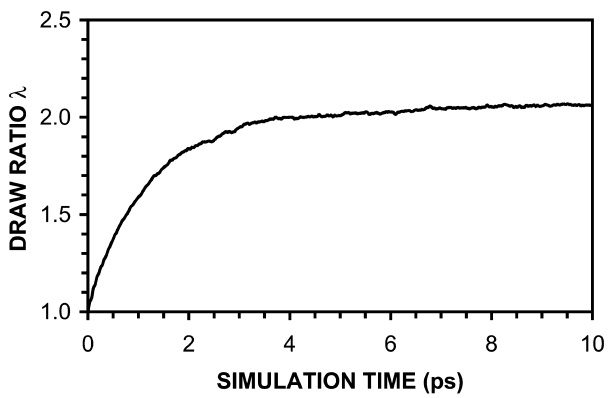

Fig. 1. Evolution of deformation under Parrinello–Rahman conditions ($S_{xx} = 0.5$ GPa).

The 'cell mass' w has been proposed to be of the order of magnitude of V/c, where V is the cell volume and c the speed of sound in the material simulated [13]. As Li, Johnson and Goddard [26] have pointed out, the value of c is often not known, and trial and error must be used to ascertain reasonable boundaries for this parameter. Values ranging from 20 to 1000 were tested without any notable effect on the orientation, as measured by $\langle P_2(\cos\theta)\rangle$, whereas, the time needed to attain a reasonable deformation ratio increases substantially with increasing w. For example, at a value of w of 1000, deformation was negligible even after a 3000 fs simulation. Changes in temperature control method gave comparable results. For subsequent calculations, a value of 20 was selected, which allowed rapid calculations while allowing sufficient time for convergence.

As the cell is deformed, periodic boundary conditions lead to shorter interchain distances and more short contacts. Energies change consequently and, during the dynamics procedure, atoms move on the potential energy curve of this deformation, normally concentrating near minimum energy pathways. Energy added to the system via the applied stress allows energy barriers to be surmounted, however, and induce considerable conformational changes necessary to align the molecule along the deformation direction. Although this procedure is considerably different from experiment, forces acting on the molecules should be roughly the same, i.e. interchain interactions and conformational energy barriers. In this context, electrostatic energies are not expected to modify substantially the deformation process, as these will mostly result in repulsion of ester groups between adjacent chains. They would, however, play a crucial role during relaxation simulations, as lateral organisation would evolve to lead to crystalline domains [27].

Third, the deformation scheme used here is close to a pultrusion deformation, coupling an elongational deformation with symmetrical compression stress, cylindrical for pultrusion while in two orthogonal directions in the present simulation. This deformation scheme was used because of density fluctuation problems encountered during deformation, of the type observed previously for polyvinyl phenol orientation simulations [1], although much less severe in the present case. Lateral forces were used to help maintain density while remaining within reasonable calculation times. Nevertheless, interestingly, no noticeable changes in orientation were noted when comparing simulations performed with lateral stresses of zero to 0.5 GPa. Further, relaxation of the models after deformation did not change the orientation functions, contrarily to the case of polyvinyl phenol. It is therefore, proposed that the density problems are due to difficulties in restoring lateral interchain interactions in amorphous cells. It must be also noted that changes in w were tested but did not permit to alleviate the

density problems. As long as the magnitude of the lateral stresses did not exceed that of positive deformation stress, orientation remained uniaxial, as testified by the fact that, for a deformation in the x direction, the values of $\langle P_2(\cos\theta)\rangle_x = -0.5\ \langle P_2(\cos\theta)\rangle_y = 0.5\ \langle P_2(\cos\theta)\rangle_z$, where $\langle P_2(\cos\theta)\rangle_i$ is the orientation function as measured when the reference direction is the i axis. Temperature control was performed, for most runs, using the velocity rescaling technique. It allows the use of larger timesteps, and is thus much faster. Prior to selecting this method, a few runs were made using an alternate temperature scheme proposed by Nosé. Resulting models were similar both in terms of resulting orientation and conformation distribution. Deformation runs were also performed at temperatures varying from 25 to 225 °C, and no changes in orientation or conformer distribution were noted neither under these conditions. It was, therefore, concluded that temperature control was not a sensitive parameter in deformation simulations when investigating orientation and conformation population, and that faster but less precise velocity rescaling could be used.

The initial amorphous model ($\lambda = 1.0$) and one of the deformed models ($\lambda = 3.5$) are depicted in Fig. 2(a) under periodic boundary conditions. As can be seen, the structures are densely packed, and although hydrogen atoms are omitted, details of the molecular structure are difficult to ascertain. It is easier to visualize the PET chain before it is folded back into a single unit cell, as shown in Fig. 2(b). As expected, as deformation proceeds, segments are more and more aligned with the deformation direction, which coincides with the unit cell long axis. Sections which are well extended grow in length and in conformational regularity. At a λ of 3.5, sections which are seen as folding in a single, continuous chain are proposed to be participating in chain entanglements with other neighbouring chains, which limits their extension. Deformations up to λ of 4.0 were performed. For higher draw ratios, the unit cell showed deviations from orthogonality, caused by deviations from zero of the off-diagonal stress tensors. These could be related to violations in the minimum image convention or, alternatively, to local internal energy variations.

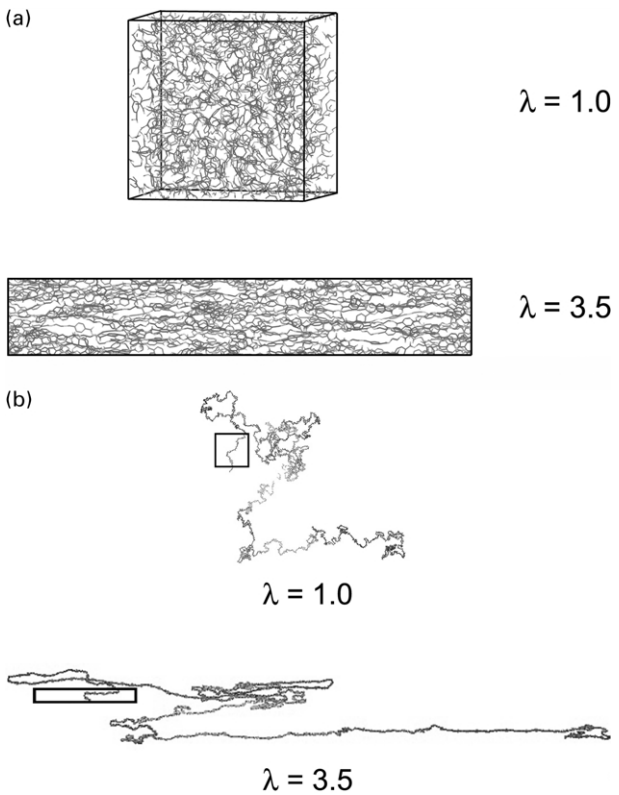

Fig. 2. Amorphous phase model (hydrogen atoms omitted for clarity). (a) Content of unit cell under periodic boundary conditions. (b) One continuous chain with respect to defined unit cell.

3.3. Orientation calculations

The orientation distribution of polymer segments can be fitted with a Legendre polynomial series. For uniaxial orientation, the coefficients of the first term of this series, $\langle P_2(\cos\theta)\rangle$,

$$\langle P_2(\cos\theta)\rangle = \tfrac{1}{8}\langle 30\cos^2\theta - 1\rangle \quad (1)$$

where θ is the angle between the local chain axis of the segment under consideration and the reference direction (which is usually taken as the deformation direction), and $\langle\ \rangle$ indicates an average over all segments. $\langle P_2(\cos\theta)\rangle$ can be obtained via many experimental techniques, the most widely employed being birefringence and infrared dichroism. The second term of this series, $\langle P_4(\cos\theta)\rangle$,

$$\langle P_4(\cos\theta)\rangle = \tfrac{1}{8}\langle 3 - 30\cos^2\theta + 35\cos^4\theta\rangle \quad (2)$$

can be obtained by Raman spectroscopy, whereas, NMR and X-ray diffraction can yield as well higher order terms. Limiting values for $\langle P_2(\cos\theta)\rangle$, which is the most commonly used orientation function, are of 1 for perfect uniaxial orientation along the reference direction, 0 for isotropic samples and -0.5 for perfect orientation perpendicular to the reference direction.

Orientation calculations were performed for *trans*, *gauche* and aromatic cycles. An alternate subdivision in *trans* and non-*trans* angles was also used, as it was suspected that the infrared *gauche* vibration may encompass a larger variety of conformations. The exact chain segments used to calculate the orientation are depicted in Fig. 3. The aromatic cycle orientation has been defined as the average of the orientation of the two C–C bonds of the aromatic cycles which lie parallel to the C–C bonds attaching the aromatic moiety to the ester function. As this moiety is not divided in subclasses, it will be used as an indication of the overall orientation of the polymer and will be referred to as $\langle P_2(\cos\theta)\rangle_c$ throughout the text. For the aliphatic segment orientation of *trans*, *gauche* and non-*trans* subpopulations,

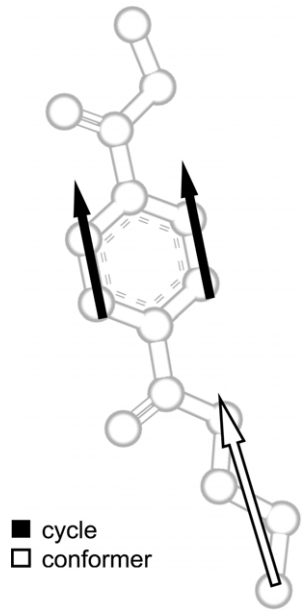

Fig. 3. Definition of atomic vectors for orientation calculation.

the vector passing through the sp^3 oxygen atoms of the glycol moiety was used.

Values of $\langle P_2(\cos\theta)\rangle_c$ as a function of λ are reported in Fig. 4. Increases in S_{xx} were used to allow the system to reach higher draw ratio. As can be seen in the figure, these did not induce any significant change in orientation. A gradual, slightly non-linear increase of $\langle P_2(\cos\theta)\rangle_c$ with respect to λ is observed. Smaller stresses were preferred for lower λ values because of practical considerations in terms of sampling during the simulation. In the first stages of the calculations, deformation proceeds very fast, thus requiring small time sampling intervals. Since, for small stresses, the maximum λ value is reached relatively fast, this does not cause any problem. For higher stresses, where higher λ values are reached, such small time sampling intervals would have resulted in enormous files. In this case, larger sampling intervals were used. Therefore, data points reported in graphs of λ versus conformation or orientation invariably incorporate data points from many different stresses. Temperatures were varied for a series of deformation under the same stress tensors using the same amorphous phase model. All temperatures resulted in the same $\langle P_2(\cos\theta)\rangle_c$ versus λ behaviour.

3.4. Conformer evolution

Fig. 5 reports different conformer populations calculated with deformation. *Trans* conformers are more than twice as frequent as true *gauche* angles. As deformation proceeds, the number of *trans* conformers increases steadily, reaching 50% for a deformation ratio of 3.2. Both the *gauche* and non-*trans* conformers decrease in a similar fashion during deformation. As mentioned previously, experimental data only allow the distinction between two conformer populations, which are usually labelled *trans* and *gauche*, although the latter are believed to correspond to non-*trans*. In Fig. 6, the experimental data of Cunningham et al. [20] were also added for comparison purposes, and the fit between the present simulation and their data is, as can be seen, very good.

Upon deformation, all authors agree upon a significant and gradual increase in *trans* conformer population, although the extent of this increase varies with the experimental technique used and measurement conditions. Data from Spiby, O'Neill, Duckett and Ward [21] agree with the values of 44% found in the simulations for $\langle P_2(\cos\theta)\rangle_c = 0.4$ at $\lambda = 2.0$ and, to a lesser extent, with data from Ajji, Cole, Dumoulin and Brisson [2] (20% *trans* at a $\lambda = 2.0$). The general trend is always the same: an increase in *trans* segment up to a 50% content for a λ of 4–5.

Similarly, the simulations by Zhou, Nicholson, Davies and Ward [7] show a steady increase in the *trans* content up

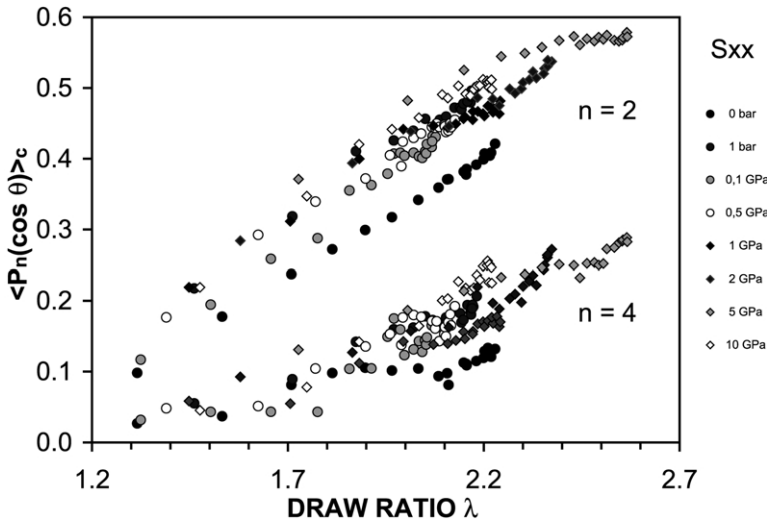

Fig. 4. Orientation factor $\langle P_n(\cos\theta)\rangle_c$ at different deformation ratios λ (n indicates the 2nd or 4th moment of the orientation function).

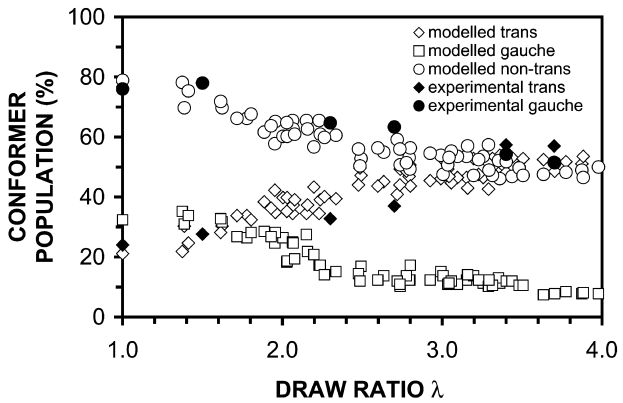

Fig. 5. Conformer population changes during deformation (using stresses of 0.5, 5.0 and 12.0 GPa).

to approximately 70% for a $\langle P_2(\cos\theta)\rangle$ value of 0.7 (of the benzene ring), as compared to 50% in the present study. The distinction between *gauche* and non-*trans* segments is proposed to be responsible for the difference observed between the two different simulations. PVPh simulations also indicate a steady increase in *trans* torsion angles with orientation, whereas, the *gauche* population decreases. Relative percentages of *trans*, *gauche* and non-*trans*–non-*gauche* angle were different in this case, as expected from the different unit cells and, therefore, the different conformer populations prior to deformation.

3.5. Conformer and aromatic ring orientation

The orientation of different conformer population is not the same, as can be seen in Fig. 6. The orientation of the cycles, $\langle P_2(\cos\theta)\rangle_c$, lies between those of *trans* and *gauche* conformers, although it is closer to *trans* values, which is the major conformer in highly deformed samples. As orientation of the cycles is conformation-independent, it can be taken as an indicator of the overall or global orientation of the polymer chain.

Table 1 gives a summary of the main references dealing with uniaxial orientation of amorphous PET, both in terms

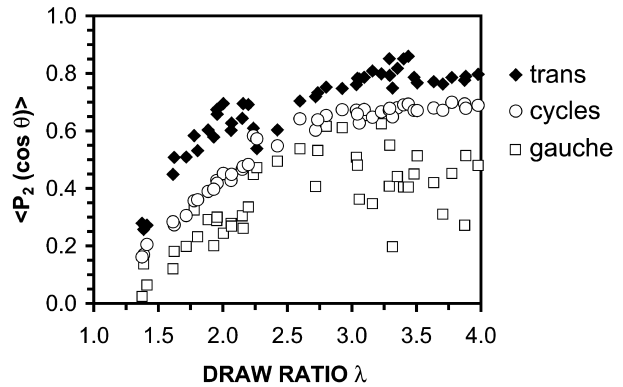

Fig. 6. Orientation of *trans*, *gauche* and non-*trans* segments during deformation under stresses of 0.5, 5.0 and 12.0 GPa (experimental data shown taken from Ref. [20]).

Table 1
Comparison of orientation factors $\langle P_2(\cos\theta)\rangle$ for PET

	$\lambda = 1.5$	$\lambda = 2.0$	$\lambda = 2.7$
Overall orientation			
Kaito, Nakayama and Kanetsuna [35]	0.01	0.06	0.48
Cunningham, Ward, Willis and Zichy [20]	0.071	0.26[a]	0.264
Ajji, Brisson, Cole and Dumoulin [2]	0.02	0.05	0.10–0.13
Cole,Guèvremont, Ajji and Dumoulin [36]	0.04	0.06	0.34–0.48
Duchesne et al. [4]	0.18[b]	0.25[c]	–
Simulation (aromatic cycles, Zhou, et al. [7])	0.30	0.52	0.59
Simulation (aromatic cycles, this work)	0.25	0.40	0.6
Trans orientation			
Ajji, Brisson, Cole and Dumoulin [2]	0.2	0.4	0.7
Nobbs, Bower and Ward [37]	≈0.2	≈0.3	≈0.5
Duchesne et al. [4]	0.15[c]	0.25[c]	–
Simulation (this work)	0.4	0.6	0.75
Gauche orientation			
Duchesne et al. [4]	0.02[c]	0.03[c]	–
Simulation (this work)	0.1–0.15	–0.25	0.4

[a] $\lambda = 2.3$.
[b] $T_{draw} = 85$ °C, $v_{draw} = 95$ cm/min.
[c] $T_{draw} = 85$ °C, $v_{draw} = 10$ cm/min.

of experimental data and of modelling simulations. When comparing with literature experimental data, care must be taken to ascertain that reported values correspond to amorphous samples, as crystalline samples are invariably much more oriented. Since PET undergoes deformation-induced crystallization, comparisons are limited to a maximum λ of 2.7 and, even within that range, crystallization can occur [2]. As seen in Table 1, considerable variations are found among literature data, which may be due to the experimental technique used, deformation rate and temperature, crystallization onset, or choice of vibration for orientation determination. However, the observed values are systematically inferior to those obtained in the simulations, as expected from the limited relaxation in the latter. It must be recalled that experimental samples are not only stretched much more slowly, but also experience post-deformation relaxation during the time lapse between the end of stretching and quenching (or measurement in the case of dynamical methods such as modulation polarisation infrared linear dichroism). This time lapse can easily reach a few seconds, which is of the same order of magnitude as the first relaxation time observed for orientation relaxation, and considerable relaxation is known to occur under these conditions [3,4]. However, the simulation period is much shorter than that and very little relaxation is likely to occur.

For all experimental data reported, general observed trends correspond to those found in the present simulations:

trans segments orient more that the overall chain, or than *gauche* segments, and orientation reaches a plateau near a draw ratio of 3.0–4.0.

The orientation of non-*trans* segments is of particular interest. Most data reported in the literature do not report any measurable orientation for the *gauche* segments. Polarization–modulation infrared linear dichroism, which allows faster and more precise measurements, does yield a small but non-negligible orientation [4]. Simulations give considerably higher orientation values. Polarisation–modulation infrared linear dichroism measurements indicate that, in the time frame accessible by this technique, all segments relax in a similar fashion [4]. Therefore, it is proposed that this difference in orientation of the two types of segments originates from intrinsic differences in orientation of *gauche* and *trans* conformers and not from differences in post-deformation relaxation, in agreement with the present simulations.

Since relaxation is normally much more limited in molecular modelling deformation simulations, a better fit is expected, quantitatively, when comparing modelled data. This is indeed what is observed when comparing the present study to that reported by Zhou et al. [7]. The most striking resemblance is the non-linearity of $\langle P_2(\cos\theta)\rangle_c$ versus λ. The actual values reported by Zhou et al. are slightly higher than those of the present study, but remain very close as compared to experimental values. Possible causes in the deviations observed between the two simulations include the type of deformation performed as well as chain length and molecular weights.

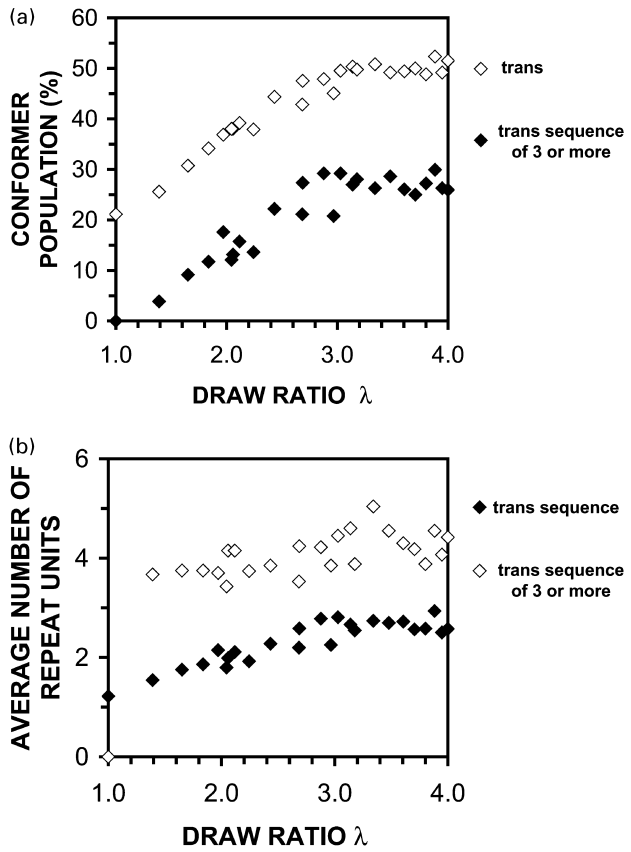

Fig. 7. Evolution of *trans* segments in deformation model under stresses of 0.5, 5.0 and 12.0 Gpa. (a) Percentage of *trans* segments belonging to *trans* sequences. (b) Average number of repeat units per *trans* sequence.

3.6. Deformation and size of crystallizable segments

It is interesting to note that, whereas, the *trans* torsion angles were distributed almost randomly in the initial isotropic model, as deformation proceeds, the *trans* sequence length increases steadily in some sections of the chain. This is compatible with the occurrence, in actual experimental conditions, of deformation-induced crystallization. These *trans* chain portions become slowly parallel as orientation proceeds, as testified by the higher $\langle P_2(\cos\theta)\rangle$ values of *trans* segments both in the present deformation models and in experimental data. Van der Waals and electrostatic interchain interactions undoubtedly favour the minimum energy packing, that of the crystalline phase. In the literature, two approaches, namely the theory of 'cold' crystallization proposed by Wunderlich [28], and a combination of molecular modelling and experimental melting point depression [29], yielded a minimum number of sequences for participating in crystallite formation at three for PET. As it is known that PET adopts a *trans* conformation in the crystal structure, it is possible to investigate incipient crystallization by following the persistence of *trans* conformers.

As can be seen in Fig. 7(a), for obvious statistical reasons, the total percentage of *trans* conformers is always larger than that of *trans* conformers belonging to triads or to longer *trans* sequences. The number of *trans* segments reaches a plateau in both cases around a λ of 2.0–2.5, which is the draw ratio near which deformation-induced crystallization occurs [2]. The length of *trans* sequences increases steadily upon deformation, as seen in Fig. 7(b). On the other hand, the length of *trans* sequences of more than 3 repeat units varies much less within the studied deformation ratios, which is compatible with a random occurrence of *trans* segments, which will event contribute to both increasing the length of existing segments and form new ones.

No regular lateral packing or order could be detected through visual inspection, contrarily to that observed in a simulation of polyethylene by Lavine, Waheed and Ruthledge [27]. Further, as can be seen in Fig. 8, the interchain atomic pair distribution function $g(r)^{inter}$ does not show the presence of any peaks which would have been the sign of ordering of the structures. It has been shown that the occurrence short-range order similar to crystallization depends largely on the forcefield use, and more specifically on the torsional energy terms used. However, in the present case, contrarily to polyethylene, crystallization may also occur on a longer time scale than deformation. This is in agreement with polarisation modulation infrared linear dichroism experiments which show that, at a draw ratio of

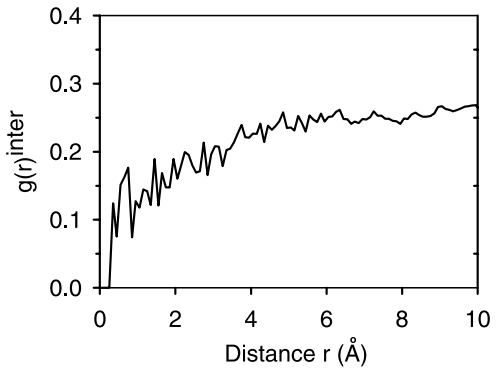

Fig. 8. Interchain pair distribution function $g(r)^{inter}$ for the model stretched to $\lambda = 3.5$.

2.0, no recrystallization occurs at 85 °C whereas, at a temperature of 100 °C, orientation is followed first by a relaxation process, resulting in a decrease in the orientation factor, and then by a rapid increase in orientation [4]. This increase is accompanied by an increase in the *trans*/*gauche* ratio, and has been shown by differential scanning calorimetry measurements to be related to an increase in crystallinity The time-scale of this crystallization procedure is around 250 s, well outside of the realms of atomistic molecular dynamics simulations. The *trans* chain segment portions of the present deformation models should be though of as possible nucleation sites for crystallization or pre-crystalline domains.

3.7. Comparison with affine and non-affine models

Although numerous theories have been proposed to explain the deformation behaviour of polymers, perhaps the most common ones are the network rubber elasticity or affine model and the aggregate or pseudo-affine model (Fig. 9).

In a rubberlike network, the polymer is assumed to be a network of freely joined chains composed of identical links, as proposed initially by Kuhn and Grün. These links are connected at entanglements points in amorphous polymer

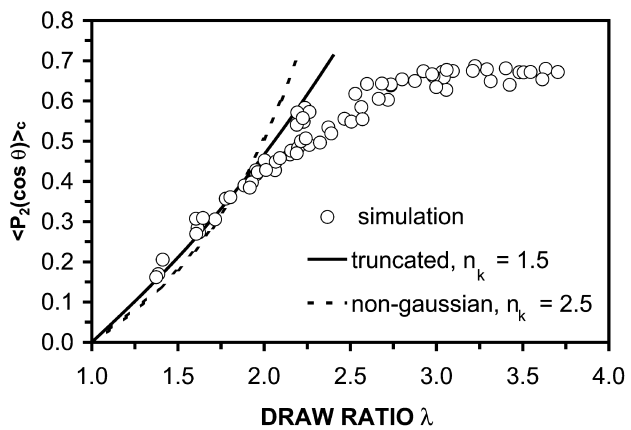

Fig. 9. Comparison of molecular dynamics simulation and of the rubber elasticity network deformation model.

systems and experience an affine deformation of junction points. At low deformation, the orientation function can then be given, to a first approximation, by:

$$\langle P_2(\cos\theta)\rangle = \frac{1}{5n_k}\left(\lambda^2 - \frac{1}{\lambda}\right) \tag{3}$$

where n_K is the number of Kuhn segments between entanglements. The inclusion of non-gaussian terms (which should have minimal effect for large entanglement spacings) results in the following equation:

$$\langle P_2(\cos\theta)\rangle = \frac{1}{5n_k}\left(\lambda^2 - \frac{1}{\lambda}\right) + \frac{1}{25n_k^2} \times\left(\lambda^4 - \frac{\lambda}{3} - \frac{4}{3\lambda^2}\right) + \frac{1}{35n_k^3} \times\left(\lambda^6 - \frac{3\lambda^2}{5} - \frac{8}{5\lambda^2}\right) \tag{4}$$

A second deformation model was proposed by Kratky [30] for semi-crystalline polymers. It has, however, been developed in more details and applied to amorphous polymers under the name of the aggregate model by Ward [31]. In this model, the deformation is proposed to occur through tilting of rigid segments towards the deformation axis. It neglects changes in the length of the units upon deformation and is, therefore, sometimes called the pseudo-affine model. In this case, the orientation factor is related only to the draw ratio through the following equation [31]

$$\langle P_2(\cos\theta)\rangle = \frac{1}{2}\left\{\frac{2\lambda^3+1}{\lambda^3-1} - \frac{3\lambda^3\cos^{-1}\lambda^{-3/2}}{(\lambda^3-1)^{3/2}}\right\} \tag{5}$$

An expression for $\langle P_4(\cos\theta)\rangle$ was likewise developed [32]. Both the affine and the aggregate models include a dependence of $\langle P_2(\cos\theta)\rangle$ on deformation ratio λ. The nature of the repeat unit is however neglected in the aggregate model, while it is taken into account via the value of n_k in the affine model.

As can be seen in Fig. 8, the $\langle P_2(\cos\theta)\rangle$ versus λ curve shows a reasonable fit with the affine model (not including Gaussian terms) up to a λ of 2.0. Linear regression yields a n_k value of 1.5. The fit including non-gaussian terms is not as good, and results in a slightly higher n_k value of 2.5, as seen on Fig. 8 as a dashed line. This is not surprising, as in the present case, the entanglement spacing can be estimated as being between 47 and 53 nm from experimental data on M_e and $\langle R_o\rangle^2/M$. These values we used previously in the present article to estimate the number of Kuhn segments between entanglements, which is of 31, and the length per Kuhn chain, which is of 1.5–1.7 nm. The entanglement spacing is therefore long enough for the Gaussian approximation to apply.

The fit at low draw ratios is therefore in agreement with the affine model, without having to incorporate non-Gaussian terms, for small draw ratios. Similar fits were

observed in the PVPh simulations, up to comparable draw ratio of 2.0 [1]. A more objective way to ascertain the linearity domain is to draw the $5\langle P_2 \cos\theta\rangle$ versus $(\lambda^2 - 1/\lambda)$ curve, which should yield a linear relationship with slope equal to $1/n_k$. As can be seen in Fig. 10, this approach yields a linear relationship up to a λ of 2.0 ($\lambda^2 - 1/\lambda = 3.5$).

Experimentally, Cunningham, Ward, Willis and Zichy [20] observed that PET follows the rubberlike network model up to a draw ratio of 4, after which the behaviour tends towards that of the aggregate model observed. They derived, using polarised infrared spectroscopy, a value of n_k of approximately 5, whereas, stress-optical data yielded a value of n_k of 6 [33]. This discrepancy is attributed to the presence of relaxation under the experimental conditions. In most deformation procedures, the sample size is held constant while quenching is performed. During this time, significant relaxation occurs, which decreases the observed orientation. The draw ratio however stays the same. Using such quenched data invariably leads to a decrease in the slope of orientation versus draw ratio and, therefore, to a decrease in the experimentally determined n_k value, as compared to that which would have been observed without relaxation. Confirmation that the fit of this model is relaxation-dependent is the observation by Padibjo and Ward [34] that the limiting draw ratio for rubber elasticity behaviour increases with draw temperature. Experimental n_k values are probably underestimated because of relaxation, but is the simulation value, which is close to one, realistic? Possibly not. It can be argued that simulation deforms the chain more drastically than could be done experimentally without sample breakage and, therefore, that values obtained in the simulations do not represent the steady-state equilibrium, contrary to what is required for the rubber elasticity model. It might be more appropriate to relax the deformed cells and to derive a n_k value afterwards, although to what extent this is necessary is difficult to establish.

In the simulations, the observation of a n_K value close to unity indicates that the deformation proceeds as if each repeat unit was a rigid segment, the flexible O–C–C–O bond being the junction point between two adjacent segments and permitting conformational changes necessary to cause segment realignment along the deformation direction. This description strongly points to the aggregate model. In Fig. 10 are reported the orientation factors $\langle P_2(\cos\theta)\rangle_c$ and $\langle P_4(\cos\theta)\rangle_c$ of deformation models, along with calculated values using the aggregate model, which appear as solid lines. A good agreement is observed for $\langle P_2(\cos\theta)\rangle_c$, and an acceptable one for $\langle P_4(\cos\theta)\rangle_c$. As mentioned previously, simulations by Zhou, Nicholson, Davies and Ward yielded a similar fit, with slightly higher orientation factors [7] (Fig. 11).

The observed agreement between simulations and the aggregate model is unexpected, as experimental values previously reported in the literature fitted with the model only at high deformation ratios. A possible cause could be that, at such deformation ratios, incipient crystallization may hinder relaxation, thus maintaining orientation closer to the values originally achieved and, therefore, explaining the agreement in this range.

However, this behaviour completely differs from that of PVPh simulations, which gave orientation values lower than those predicted by the aggregate model, the discrepancy being small for *trans* segments, but reaching a factor of 2 for backbone orientation, and a factor of 3 for *gauche* segments. This is even more striking when considering that initial *trans* population, whose behaviour is closer to the aggregate model, is higher by almost a factor of two in PVPh as compared to PET. PVPh is similar to polystyrene, although it bears a hydrogen bond forming hydroxyl group in the para position of the aromatic ring. The phenol substituent considerably rigidifies the chain by increasing rotational barriers. However, the backbone itself is composed solely of a methylene chain. The relative number of flexible segments that undergo conformational changes from *gauche* to *trans* and, therefore, that undergo a change in relative length (not taken into account in the aggregate model) is higher in PVPh than in PET, in which the backbone is composed both of flexible glycol moities and of rigid terephthalate units. In this sense, chain rigidity is higher in

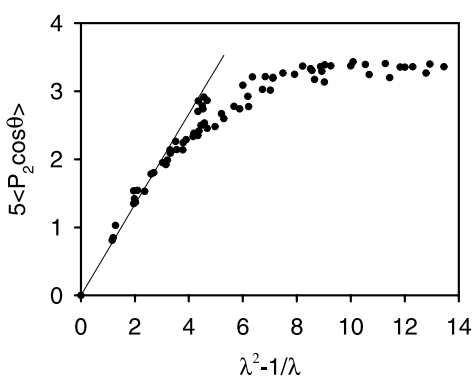

Fig. 10. Determination of the linearity domain for the rubber elasticity model.

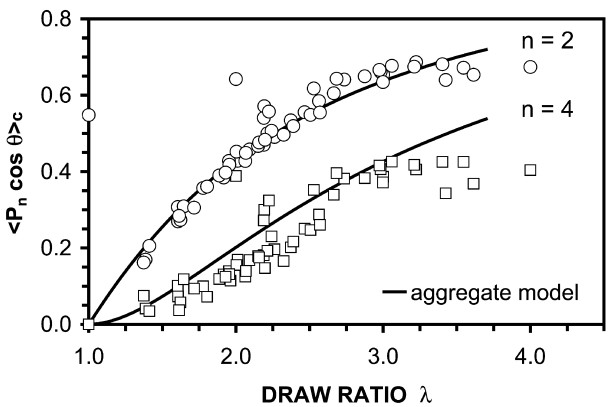

Fig. 11. Comparison of molecular dynamics simulation and of the aggregate model for $\langle P_2(\cos\theta)\rangle$ and $\langle P_4(\cos\theta)\rangle$ orientation factors.

PET, and the pseudo-affine approximations hold better, hence its better fit with the aggregate model.

4. Conclusion

In the present paper, simulation of PET orientation is reported. Modelled data fit the predictions of the aggregate model for orientation of the cycles and of the *trans* glycol segments, whereas orientation of *gauche* segments is considerably lower. This behaviour is different from that of previously modelled PVPh, for which orientation values were significantly lower that the aggregate model predictions for overall and *gauche* segments, while *trans* segment conformed to the predictions. This is proposed to stem from the affine prediction used in the aggregate model, which is appropriate for *trans* segments and for relatively rigid backbone polymers such as PET. For the more flexible PVPh backbone, which is only composed of aliphatic segments, and for *gauche* angles, this approximation appears to introduce non-negligible deviations from the predictions. Modelling, therefore, clearly shows chain flexibility, which has been relatively neglected so far in orientation studies, is a key factor in the final orientation of polymers.

Acknowledgements

The authors wish to acknowledge the financial support of NSERC (Natural Science and Engineering Research Council of Canada) and of the FCAR (Fonds pour la formation des chercheurs et l'aide à la recherche, Gouvernement du Québec) for financial support.

References

[1] Gestoso P, Brisson J. J Polym Sci Polym Phys 2002;40:1601.
[2] Ajji A, Brisson J, Cole KC, Dumoulin MM. Polymer 1995;36:4023.
[3] Oultache K, Kong X, Pellerin C, Brisson J, Pézolet M, Prud'homme RE. Polymer 2001;42:9051.
[4] Duchesne C, Kong X, Brisson J, Pézolet M, Prud'homme RE. Macromolecules 2002;35:8768.
[5] Hedenqvist MS, Bharadwaj R, Boyd RH. Macromolecules 1998;31:1556.
[6] Ward IM, Bleackley M, Taylor DJR, Cail JI, Strepto RFT. Polym Engng Sci 1999;39:2335.
[7] Zhou J, Nicholson TM, Davies GR, Ward IM. Comput Theor Sci 2000;10:43.
[8] Maple JA, Hwang M-J, Stockfisch TP, Dinur U, Waldman M, Ewig CS, Hagler AT. J Comput Chem 1994;15:162.
[9] Hwang M-J, Stockfisch TP, Hagler AT. J Am Chem Soc 1994;116:2515.
[10] Sun H. J Comput Chem 1994;15:756.
[11] Meirovitch H. J Chem Phys 1983;79:50.
[12] Huai S, Rigby D. Spectrochim Acta 1997;A53:1301.
[13] Parrinello M, Rahman A. J Appl Phys 1981;52:7182.
[14] Theodorou DN, Suter UW. Macromolecules 1985;18:1476.
[15] McAlea KP, Shultz JM, Garner KH, Wignall GD. Macromolecules 1985;18:447.
[16] Williams AD, Flory PJ. J Polym Sci 1967;5:417.
[17] Wallach ML. Macromol Chem 1967;103:79.
[18] Aharoni SM. Macromol Chem 1978;179:1867.
[19] Rigby D. Polymer 1978;19:1229.
[20] Cunningham A, Ward IM, Willis HA, Zichy V. Polymer 1974;15:749.
[21] Spiby P, O'Neill MA, Duckett RA, Ward IM. Polymer 1992;33:4479.
[22] Heffelfinger J, Schmidt PG. J Appl Polym Sci 1965;9:2661.
[23] Shen D, Long F, Wen Z, Qian R. Macromol Chem 1991;192:301.
[24] Guèvremont J, Ajji A, Cole KC, Dumoulin MM. Polymer 1995;36:2285.
[25] Rodriguez-Cabello JC, Merino JC. J Appl Polym Sci 1996;62:1953.
[26] Li M, Johnson WL, Goddard III WA. Mater Res Soc Symp Proc 1993;291:285.
[27] Lavine MS, Waheed N, Ruthledge GC. Polymer 2003;44:1771.
[28] Wunderlich B. J Chem Phys 1958;29:1395.
[29] Madkour TM, Barakat AM. Comput Theor Polym Sci 1997;7:35.
[30] Kratky O. Kolloid Zeitschrift 1933;64:213.
[31] Ward IM. Proc Phys Soc 1962;80:1176.
[32] Ward IM. J Polym Sci, Polym Symp 1977;58:1.
[33] Pinnock PR, Ward IM. Trans Faradau Soc 1966;62:1308.
[34] Padibjo SR, Ward IM. Polymer 1983;24:1103.
[35] Kaito A, Nakayama K, Kanetsuna H. J Polym Sci, Polym Phys 1988;26:1439.
[36] Cole KC, Guèvremont J, Ajji A, Dumoulin MM. Appl Spectrosc 1994;48:1513.
[37] Nobbs JH, Bower DI, Ward IM. J Polym Sci, Polym Phys 1979;17:259.